Turkish Journal of Electrical Engineering & Computer Sciences

http://journals.tubitak.gov.tr/elektrik/

Research Article

Turk J Elec Eng & Comp Sci
(2020) 28: 1871 – 1885

doi:10.3906/elk-1908-163

Multiplicative-additive despeckling in SAR images

Gülay AKSOY[1], **Fatih NAR**[1,*]
[1]Department of Computer Engineering, Konya Food and Agriculture University, Konya, Turkey

Received: 29.08.2019 • **Accepted/Published Online:** 06.03.2020 • **Final Version:** 29.07.2020

Abstract: Visual and automatic analyses using synthetic aperture radar (SAR) images are challenging because of inherently formed speckle noise. Thus, reducing speckle noise in SAR images is an important research area for SAR image analysis. During speckle noise reduction, homogeneous regions should be smoothed while details such as edges and point scatterers need to be preserved. General speckle noise model contains gamma distributed multiplicative part which is dominant and Gaussian distributed additive part which is in low amount and mostly neglected in literature. In this study, a novel sparsity-driven speckle reduction method is proposed that takes both multiplicative noise model and additive noise model into consideration. The proposed speckle reduction method uses a cost function with multiplicative and additive data terms besides the total variation smoothness term. Also, an efficient and stable numerical minimization scheme is proposed for the proposed cost function that deals with multiplicative and additive noise. Speckle reduction performance of the proposed method is shown on synthetically generated SAR images and real-world SAR images.

Key words: Synthetic aperture radar, despeckling, variational methods, general speckle model, multiplicative gamma noise, additive Gaussian noise

1. Introduction

One of the most important features of life on our planet is its incredible diversity and constant change in this diversity because of natural forces and human kind. Many areas such as oceans, lakes, rivers, lands, forests, natural resources, urban areas and military areas are constantly changing. Evaluation of these changes is of great importance in our future, but monitoring the changes that have mentioned inherently contains many challenges. Many remote sensing methods and systems have been developed to overcome such challenges by allowing us to observe the earth surface. Among various remote sensing systems, optical systems and radars are the most important ones. Comparing SAR and optical remote sensing, SAR has some advantages, such as getting data in all weather [1]. However, SAR images are degraded by granular pattern fused on the actual SAR signal called speckle, which is a variation of pixel reflectivity [2]. The source of speckle pattern, which is in a granular form, is the existence of multiple scatterers in a resolution cell inherent in SAR imaging systems. One example of quality degradation is not having a constant radiometric level in homogeneous areas because of speckle pattern, that is also called as speckle noise [3]. The performance of information extraction applications using SAR images may diminish as speckle noise level increases [4].

*Correspondence: fatih.nar@gidatarim.edu.tr

1.1. Overview of speckle noise

Speckle noise is formed due to the multiple scatters in a scene formed in an image cell and has the characteristics of multiplicative noise. It has a granular form due to diffuse scattering's result, which is difficult to remove [1, 5]. Although the multiplicative component in speckle noise is dominant, SAR systems also contain a low amount of additive noise [2]. The general form of speckle noise in SAR images is given in Equation 1:

$$g = fn_{multiplicative} + n_{additive}, \tag{1}$$

where g is the noisy SAR image, f is the noise-free SAR image, $n_{multiplicative}$ is the multiplicative noise due to coherent interference, and $n_{additive}$ is the additive noise due to sensor noise. The speckle noise model is most appropriate and accurate noise model for SAR imaging that has been proven so far [2].

1.2. Speckle reduction approaches

In the SAR literature, various methods are proposed to reduce speckle noise while preserving the image details such as edges, point scatterers, and textures. These despeckling methods can be divided into 6 major categories: (a) traditional (sliding window based) approaches, (b) nonlocal means (self patch similarity) based approaches, (c) transform domain (i.e. wavelet, shearlet) based approaches, (d) machine learning based (i.e. deep learning) approaches, (e) physics (i.e. diffusion) based approaches, and (f) variational approaches.

In traditional approaches, the filtered reflectivity value is calculated for each pixel using neighbour pixels in a sliding window. Mean filter, Gaussian filter, median filter, and Wiener filter [6] are among applied filters to the SAR images that are not optimal for SAR images since they are designed for optical images. Therefore, adaptive speckle reduction filters are designed which takes into account the properties of SAR images. The Frost filter [7], Lee filter [8], Kuan filter [9], modified Frost filter [10], and modified Lee filter [11] are the best known adaptive filters in that category. In 2008, the improved sigma filter [5] was proposed following the principles of Lee sigma filters to improve the performance of it. These despeckling methods do not protect details such as edges, point scatterers, and textures.

Nonlocal mean based approaches overcome these limitations using self similarities in the image [12]. These approaches provide very good performance, especially for the textured regions, since such regions contain a redundant amount of self similarities. Initially, nonlocal mean based approaches are proposed for optical images but lately nonlocal mean based SAR despeckling algorithms are also proposed such as probabilistic patch-based (PPB) [13] method and SAR-BM3D [14] method.

Transform domain techniques are also applied by researchers where denoising is applied in the transformed domain then inverse transform is applied to obtain the denoised image. Various wavelet transform (WT) based despeckling methods are proposed in [14–16]. WT converts multiplicative speckle noise into additive noise then it removes the speckle noise in the wavelet domain. Similarly, in [17] shearlet transform is used for speckle reduction in SAR images. Wavelet and shearlet transform approaches uses known basis functions for transformation, while dictionary approaches learns the basis from the image data itself. Therefore, dictionary based approaches [18, 19] combine transform techniques with unsupervised learning.

Dictionary based approaches learn a basis in an unsupervised manner. But due to the success of machine learning, supervised approaches are also proposed where noisy and noise-free image pairs are used for training [20, 21]. However, it is very difficult to obtain noise-free versions of real-world SAR images. Thus, training data are generally synthetically generated in these approaches which limits their despeckling performance.

As another approach, diffusion-based methods that are inspired from physics are also proposed. In their seminal work, Perona and Malik proposed an ansiotropic diffusion based denoising method with a spatially varying diffusion coefficient where less smoothing is applied in pixels with high gradient values since they are possible edges [22]. This development led to an extensive amount of research for various image processing tasks using linear and nonlinear diffusion processes [23]. Later, these approaches, which are originally developed for optical images, are also extended for SAR images. For example, the speckle-reducing anisotropic diffusion (SRAD) method provides speckle reduction using a Lee filter based on a partial differential equation model for anisotropic diffusion [24].

Rudin, Osher and Fatemi (ROF) [25] extend the diffusion-based approaches by introducing a data fidelity term which is called as total variation (TV) regularizer. In the ROF model, a noise reduction approach that preserves the edges by applying the ℓ_1-norm penalty to the derivatives of the reflectance values in the image is developed. This ℓ_1-norm regularization term acts as a nonlinear diffusion process, which is also called as TV diffusion. However, ROF model has an additional data fidelity term for additive Gaussian noise that enforces a solution similar to given input noisy image. As an extension of ROF model, in [26] sparsity driven despeckling (SDD) method is proposed that makes it possible to make the TV regularizer term as ℓ_0-norm, fractional norm, and ℓ_1-norm. SDD method is improved with quadratic-linear (QL) approximation for ℓ_1-norm TV regularization term which leads to better despeckling with lower execution times, namely SDD with QL (SDD-QL) [27]. In [28] Fast SDD-QL method is proposed as an efficient and simple mechanism to increase the speed of SDD-QL method up to an order of magnitude while obtaining the better despeckling result. However, ROF, SDD, SDD-QL, and Fast SDD-QL all assumes additive Gaussian noise, which limits the performance of the despeckling since speckle noise is multiplicative. Aubert et al. [29] are the first researchers who use a variational approach to reduce multiplicative noise which is assumed to be gamma distributed, the AA model. But AA model is not convex, so achieving global convergence for multiplicative noise is not guaranteed. Durand et al. [30] have preferred to take the logarithm of the reflectivities in order to convert multiplicative noises to additive noise. This approach was also used by Bioucas et al. [31]. However, as noted by Liu et al., despite this approach to convert multiplicative noise to additive noise is facilitating the solution by producing a convex cost function, the results obtained are not correct.

In this study, inspired from our earlier study in [32], the multiplicative-additive despeckling (MAD) method is proposed as an enhancement to the AA method [29]. AA method models speckle noise in gamma distributed multiplicative form where it uses an explicit numerical solver, which is not stable and lead to dithering artifacts in a despeckled image. First, MAD method employs an efficient implicit solver which is unconditionally stable so that the despeckled image is free of dithering artifacts. Second, AA method ignores the additive noise component while the MAD method models both multiplicative and additive noise components, gamma distributed and Gaussian distributed, respectively. Last, MAD method employs accurate and efficient ℓ_1-norm numerical approximation for the TV regularization term. These 3 contributions ensure preservation of the edges and point scatterers in the SAR image while smoothing homogeneous regions. Therefore, proposed MAD method provides better speckle noise reduction and better computational efficiency compared to the methods in the literature.

The remainder of the paper is organized as follows. First, Section 2 briefly explains the proposed method. Then, Section 3 presents the performance of the proposed MAD method with various experiments and comparison studies. Finally, conclusion with some remarks are given in Section 4.

2. Proposed method

Speckle reduction in a SAR image can be cast as an optimization problem where despeckled image is the solution obtained by minimizing a cost function for a given noisy image. Among the family of the cost functions, variational cost functions have desirable characteristics for preserving the details while filtering the noise. Variational cost functions contain a data fidelity term and a regularization (smoothness) term besides problem specific terms. Data fidelity term tries to enforce a solution (despeckled image) close to the given noisy image while regularization term tries to enforce smoothness on the solution so that image details such as edges and point scatterers are preserved. Proposed MAD method is expressed as a minimization of a variational cost function given in Equation 2, as an optimization problem.

$$\hat{F} = argmin\ J_{MAD}(F) \tag{2}$$

The above optimization model aims to determine the best choice of a vector that represents the speckle reduced SAR image. The variable F represents the choice made and the objective value $J_{MAD}(F)$ represents the cost of choosing F for utility. At last, cost function $J_{MAD}(F)$ is minimized with respect to F which leads to the $\hat{F}$ as a despeckled image.

2.1. Proposed cost function

The cost function $J_{MAD}(F)$ is defined as given in Equation 2, which is minimized with respect to F. This cost function can be modeled for multiplicative noise as proposed in the AA model [29] or can be modeled for the additive noise as proposed in ROF model [25]. However, general speckle noise model assumes that SAR images contain both multiplicative and additive noise where additive noise has a minor contribution. Therefore, in this study, AA model and ROF model are combined to deal with general speckle model as given in Equation 1 which contains a multiplicative noise term in addition to an additive noise term.

Proposed MAD method suggests a variational cost function with a multiplicative and an additive data fidelity terms and a TV regularization term to reduce speckle noise as given in Equation 3.

$$J_{MAD}(F) = \sum_{p}(\log F_p + \frac{G_p}{F_p}) + \lambda_a(F_p - G_p)^2 + \lambda_s|(\nabla F)_p| \tag{3}$$

where F is speckle noise reduced image, G is an image with speckle noise, the first term is a data fidelity term dictated by multiplicative noise with gamma distribution, the second term is a data fidelity term dictated by additive noise with Gaussian distribution, λ_a is a small positive constant weighting the contribution of additive noise, the third term is TV regularization term to enforce smoothness, ∇ is the gradient operator, and λ_s is a positive value, which determines the smoothing level.

2.2. Minimization of the proposed cost function

In Equation 3, the first data fidelity term, that models the multiplicative noise, is nonconvex. However, as shown in [29], in certain conditions data fidelity term for the multiplicative noise becomes convex. In addition, the absolute operator in the TV regularization term is nondifferentiable. Thus, efficient optimization of MAD cost function, especially finding the global optimum, is challenging. In this study, convex relaxation methods are used for multiplicative data fidelity term and the absolute value operator is approximated to obtain a convex and differentiable cost function which leads to an effective numerical minimization scheme.

Multiplicative data fidelity term is expanded using the first-order Taylor expansion which leads to a convex term as in Equation 4 where $\hat{F}_p$ represents a delegate constant having the same value as F_p.

$$\log(F_p) + \frac{G_p}{F_p} \approx m_p F_p + c_p \tag{4}$$

where

$$m_p = \frac{1}{\hat{F}_p} - \frac{G_p}{\hat{F}_p^2} \quad \text{and} \quad c_p = log\hat{F}_p + \frac{2G_p}{\hat{F}_p} - 1 \tag{5}$$

Despite the success of detail preservation of ℓ_1-norm TV regularization, its efficient minimization is challenging since absolute function is not differentiable. Therefore, the absolute operator is approximated using the quadratic-linear (QL) approximation approach that is suggested in [27] as below:

$$|z| \approx (1-\alpha)(|\hat{z}| + \varepsilon)^{-1} z^2 + \alpha sgn(\hat{z}) z \tag{6}$$

where the first term is a quadratic approximation, the second term is a linear approximation, α is weighting function $(0 \leqslant \alpha < 1)$ for determining the balance between quadratic and linear term, $\hat{z}$ is a surrogate constant for the value of z, and ε is a small constant value with $\varepsilon > 0$. To improve approximation accuracy, ε should be decreased as much as to 0. As seen in Figure 1, Equation 6 is accurate around 0 and the approximation point $\hat{z}$. As z decreases and converges to 0, contribution of the linear term becomes smaller and quadratic term becomes more dominant. As approximation becomes more quadratic, not only absolute function is smoothed but also staircase artifacts are also eliminated which is a common problem of ℓ_1-norm TV smoothing.

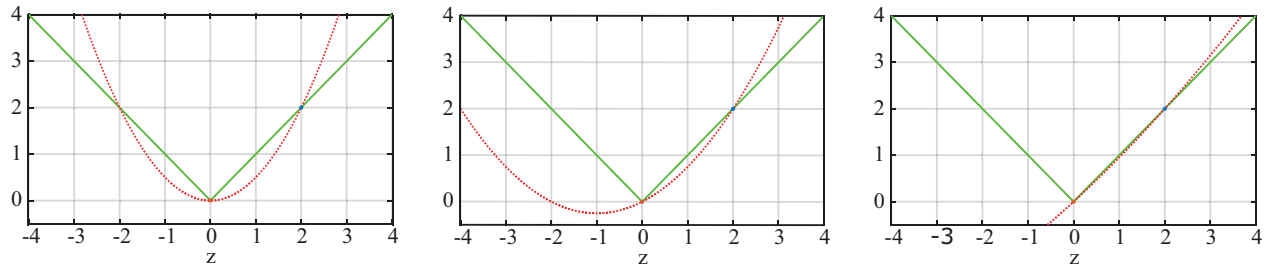

Figure 1. QL approximations for different α values ($\varepsilon = 10^{-3}$, $\hat{z} = 2$).

Since $\hat{F}_p$ is momentarily fixed and assumed to be constant, $|(\nabla F)_p|$ can be defined as below:

$$\begin{aligned} |(\nabla F)_p| &= |(\partial F_x)_p| + |(\partial F_y)_p| \\ &\approx (1-\alpha)((W_x)_p(\partial_x F)_p^2 + (W_y)_p(\partial_y F)_p^2) \\ &+ \quad \alpha((S_x)_p(\partial_x F)_p + (S_y)_p(\partial_y F)_p) \end{aligned} \tag{7}$$

where

$$(W_x)_p = (|(\partial_x \hat{F})_p| + \varepsilon)^{-1} \quad \text{and} \quad (W_y)_p = (|(\partial_y \hat{F})_p| + \varepsilon)^{-1} \tag{8}$$

and

$$(S_x)_p \approx sgn((\partial_x \hat{F})_p) \quad \text{and} \quad (S_y)_p \approx sgn((\partial_y \hat{F})_p). \tag{9}$$

Cost function given in Equation 3 is rewritten as in Equation 10 using the approximations in Equation 4 and Equation 7. Because of the applied approximations, Equation 10 is only accurate around $\hat{F}$ and is solved iteratively where superscript n in $J^{(n)}(f)$ represents the iteration index. A new regularization term $(F_p - \hat{F}_p)^2$, slow-step regularization (SSR), is added to force F_p being close to $\hat{F}_p$ since employed approximations are only accurate around $\hat{F}_p$.

$$\begin{aligned}\hat{J}^{(n)}_{MAD}(F) = &\sum_p (m_p F_p + c_p) + \lambda_a (F_p - G_p)^2 \\ &+ \lambda_s[(1-\alpha)((W_x)_p(\partial_x F)_p^2 + (W_y)_p(\partial_y F)_p^2) \\ &+ \qquad \alpha((S_x)_p(\partial_x F)_p + (S_y)_p(\partial_y F)_p)] \\ &+ \lambda_p (F_p - \hat{F}_p)^2,\end{aligned} \tag{10}$$

where λ_p is a positive weight for the SSR term. As λ_p increases numerical minimization will less deviate from the approximation point and accuracy will increase but convergence will be slower. In this study, λ_p is chosen as 1 as a good trade-off between approximation accuracy and computational efficiency.

Finally, the cost function in Equation 10 can be transformed into a matrix-vector form as below:

$$\begin{aligned}\hat{J}(V_f) = &(V_m^\top V_f + \vec{1}^\top V_c) + \lambda_a (V_f - V_g)^\top (V_f - V_g) \\ &+ \lambda_s[(1-\alpha)(V_f^\top \mathbf{C_x}^\top \mathbf{W_x} \mathbf{C_x} V_f + V_f^\top \mathbf{C_y}^\top \mathbf{W_y} \mathbf{C_y} V_f) \\ &+ \ \alpha(S_x^\top \mathbf{C_x} V_f + S_y^\top \mathbf{C_y} V_f)] \\ &+ \lambda_P (V_f - V_{\hat{f}})^\top (V_f - V_{\hat{f}}),\end{aligned} \tag{11}$$

where V_f, $V_{\hat{f}}$, V_g, V_m, V_c, S_x, and S_y symbols are vector forms of F, $\hat{F}$, G, m_p, c_p, $(S_x)_p$, and $(S_y)_p$. As a constant vector, $\vec{1}$ is formed with all ones. $\mathbf{C_x}$ and $\mathbf{C_y}$ are discrete gradient operators, and $\mathbf{W_x}$ and $\mathbf{W_y}$ are diagonal matrices for representing the $(W_x)_p$ and $(W_y)_p$. Note that vectors have the size of $k \times 1$ and matrices have the size of $k \times k$ where k represents the pixel count in the SAR image. Although, $k \times k$ is a huge matrix size even for a moderate size image (i.e. $k = 10^6$ for an image with the size of 1000×1000), all the matrices are sparse so memory and computational requirements for doing operations on these matrices become tractable. Note that, $\mathbf{C_x}$ is discrete gradient operator in x-direction and $\mathbf{C_y}$ is discrete gradient operator in y-direction where derivatives at the image boundary are zero as boundary conditions.

Minimization of Equation 11 leads to a unique global minimum since it is strictly convex. Therefore, to minimize the cost function in Equation 11, derivative of the Equation 11 is taken with respect to V_f and equalized to zero as shown in Equation 12.

$$\begin{aligned}0 = \frac{\partial \hat{J}^n(V_f)}{\partial V_f} = &V_m + 2\lambda_a (V_f - V_g) \\ &+ 2\lambda_s[(1-\alpha)(\mathbf{C_x}^\top \mathbf{W_x} \mathbf{C_x} V_f + \mathbf{C_y}^\top \mathbf{W_y} \mathbf{C_y} V_f) \\ &+ \ \alpha(\mathbf{C_x}^\top S_x + \mathbf{C_y}^\top S_y)] \\ &+ 2\lambda_P (V_f - V_{\hat{f}})\end{aligned} \tag{12}$$

After solving the Equation 12 below linear system is obtained.

$$\begin{aligned} &\mathbf{A}V_f^{(n+1)} = b \\ &\mathbf{A} = (\lambda_a + \lambda_p)\mathbf{I} + \lambda_s(1-\alpha)(\mathbf{C_x}^\top \mathbf{W_x} \mathbf{C_x} + \mathbf{C_y}^\top \mathbf{W_y} \mathbf{C_y}) \\ &b = \lambda_a V_g + \lambda_p V_{\hat{f}} - 0.5 V_m - \lambda_s(\alpha/2)(\mathbf{C_x}^\top S_x + \mathbf{C_y}^\top S_y) \end{aligned} \tag{13}$$

where $\mathbf{I}$ is the identity matrix. In case the iteration index is not explicitly stated, n is the iteration index for the $\mathbf{A}$, $\mathbf{W_x}$, $\mathbf{W_y}$, b, V_f, $V_{\hat{f}}$, S_x, and S_y. Here, $\mathbf{A}$ is a positive definite (PD) and a 5-point Laplacian matrix, which is also sparse.

In [28], the use of adaptive ε is suggested and its computational efficiency is presented. In this approach, ε is adaptively changed where ε is 1 in the first iteration and converges to the desired value as iteration proceeds. This approach is easy to implement and requires no extra computation, since it does only simple scalar computations to calculate adaptive ε (lines 3, 4, and 6 in Algorithm 1). Finally, obtained minimization approach can be implemented easily in any programming language based on the pseudo-code in Algorithm 1.

Algorithm 1 $M_{ultiplicative}A_{dditive}D_{especkling}$

1: `Inputs:` g, λ_a, λ_s, λ_p, α, $\varepsilon_{desired}$, n_{max} ▷ $\lambda_a, \lambda_s, \lambda_p > 0$, $0 \le \alpha < 1$, $0 < \varepsilon_{desired} \le 0.1$, $n_{max} > 3$
2: $V_f \leftarrow V_g \leftarrow g$ ▷ `assign image data` g `to vector` V_g `and vector` V_f `as initial solution`
3: $\varepsilon_{start} = 1$ ▷ Initial ε will be 1
4: $\varepsilon_{decrement} = \frac{\varepsilon_{start} - \varepsilon_{desired}}{n_{max}}$ ▷ `preparation for the adaptive` ε
5: **for** $n = 1 : n_{max}$ **do**
6: $\varepsilon = \varepsilon_{start} - n\varepsilon_{decrement}$ ▷ `assignment for the adaptive` ε
7: $V_{\hat{f}} \leftarrow V_f$ ▷ `assign` V_f `to proxy constant` $V_{\hat{f}}$
8: $\mathbf{W_x} \leftarrow [diag(|\mathbf{C_x} V_{\hat{f}}| + \varepsilon)]^{-1}$ ▷ $\mathbf{C_x}V_f$ `is` x`-derivative of` $V_{\hat{f}}$
9: $\mathbf{W_y} \leftarrow [diag(|\mathbf{C_y} V_{\hat{f}}| + \varepsilon)]^{-1}$ ▷ $\mathbf{C_y}V_f$ `is` y`-derivative of` $V_{\hat{f}}$
10: $S_x \leftarrow sgn(\mathbf{C_x} V_{\hat{f}})$ ▷ `signum of` x`-derivative of` $V_{\hat{f}}$
11: $S_y \leftarrow sgn(\mathbf{C_y} V_{\hat{f}})$ ▷ `signum of` y`-derivative of` $V_{\hat{f}}$
12: $\mathbf{A} \leftarrow (\lambda_p + \lambda_a)\mathbf{I} + \lambda_s(1-\alpha)(\mathbf{C_x}^\top \mathbf{W_x} \mathbf{C_x} + \mathbf{C_y}^\top \mathbf{W_y} \mathbf{C_y})$ ▷ `construct matrix` $\mathbf{A}$
13: $b \leftarrow \lambda_a V_g + \lambda_p V_{\hat{f}} - 0.5 V_m - \lambda_s(\alpha/2)(\mathbf{C_x}^\top S_x + \mathbf{C_y}^\top S_y)$ ▷ `construct vector` b
14: `solve` $\mathbf{A}V_f = b$ ▷ `calculate` V_f `for the next iteration`
15: **end for**
16: $f \leftarrow V_f$ ▷ `converts vector` V_f `to an image` f
17: `Return` f

In Algorithm 1, the computational part is solving the linear system $\mathbf{A}V_f^{(n+1)} = b$. Since $\mathbf{A}$ is PD and sparse, this linear system is efficiently solved using the preconditioned conjugate gradient (PCG) method with incomplete Cholesky preconditioner (ICP). For the PCG method, convergence tolerance and maximum iteration are set to 10^{-2} and 10^2, respectively. Note that, $\mathbf{W_x}$, $\mathbf{W_y}$ are diagonal matrices that can be kept in $k \times 1$ sized arrays, $\mathbf{C_x}$, $\mathbf{C_y}$ are discrete gradient operators that can be kept in $k \times 2$ sized arrays, and since $\mathbf{A}$ is 5-point Laplacian matrix that is symmetric it can be kept in $k \times 3$ sized array. As explained in [28], vicinity of the 0.5 is good value for α as it provides a well balanced trade-off for the accuracy, numerical stability, and computational efficiency. Thus, $\alpha = 0.5$ is used as a default value in this study.

2.3. Computational complexity analysis

For the MAD method, the computational complexity of each pseudo-code line inside the for-loop of Algorithm 1 is shown in the below Table.

Table . Computational complexity of the loop in MAD method.

Line	Code in Algorithm 1	Complexity
6	$\varepsilon \leftarrow \varepsilon_{start} - n\varepsilon_{decrement}$	$o(1)$
7	$V_{\hat{f}} \leftarrow V_f$	$o(k)$
8	$\mathbf{W_x} \leftarrow [diag(\lvert\mathbf{C_x}V_{\hat{f}}\rvert + \varepsilon)]^{-1}$	$o(k)$
9	$\mathbf{W_y} \leftarrow [diag(\lvert\mathbf{C_y}V_{\hat{f}}\rvert + \varepsilon)]^{-1}$	$o(k)$
10	$S_x \leftarrow sgn(\mathbf{C_x}V_{\hat{f}})$	$o(k)$
11	$S_y \leftarrow sgn(\mathbf{C_y}V_{\hat{f}})$	$o(k)$
12	$\mathbf{A} \leftarrow (\lambda_p + \lambda_a)\mathbf{I} + \lambda_s(1-\alpha)(\mathbf{C_x}^\top\mathbf{W_x}\mathbf{C_x} + \mathbf{C_y}^\top\mathbf{W_y}\mathbf{C_y})$	$o(k)$
13	$b \leftarrow \lambda_a V_g + \lambda_p V_{\hat{f}} - 0.5V_m - \lambda_s(\alpha/2)(\mathbf{C_x}^\top S_x + \mathbf{C_y}^\top S_y)$	$o(k)$
14	solve $\mathbf{A}V_f = b$	$O(n_{pcg_{max}}k)$

In Algorithm 1, $\mathbf{C_x}$, $\mathbf{C_y}$, $\mathbf{W_x}$, $\mathbf{W_y}$, and $\mathbf{A}$ are $k \times k$ sized sparse matrices with regular structures. Sparsity with regular structures enables reducing the computational complexity significantly. Thus, computational complexity of the lines 7-13 are reduced to $O(k)$. For line 14, PCG with ICP is used to solve $\mathbf{A}V_f = b$ where computational complexity is $n_{pcg_{max}}k$. The dominant term in lines 6-14 is $n_{pcg_{max}}k$ that are within a for-loop with n_{max} iterations. Thus, computational complexity of the for-loop becomes $o(n_{max}n_{pcg_{max}}k)$. In Algorithm 1, pseudo-code lines outside of the for-loop have computational complexity of $O(1)$ or $O(k)$. Consequently, computational complexity of the MAD method given in Algorithm 1 becomes $O(n_{max}n_{pcg_{max}}k)$. Here, n_{max} and $n_{pcg_{max}}$ are generally fixed values and determined based on the SAR image characteristics that MAD method will be executed on. Thus, it can be said that n_{max} and $n_{pcg_{max}}$ are almost a constant factor in the computational complexity. So, computational complexity analysis of the Algorithm 1 shows that proposed method has intrinsically linear execution time with respect to image size (k). As seen in Figure 2, execution time experiment is in alignment with theoretical computational complexity analysis.

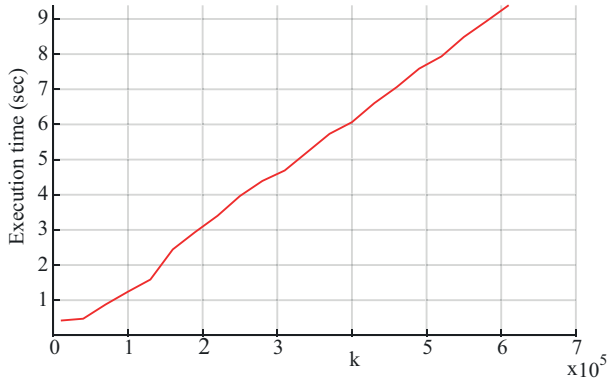

Figure 2. MAD execution time with respect to image size (k).

2.4. Convexity analysis

In this section, the convergence properties of the MAD method is analyzed theoretically and experimentally. To do so, the convexity of the cost function in Equation 11 is shown using the optimality conditions.

To satisfy the first order optimality condition, the derivative of Equation 11 is equalized to zero and a closed-form solution is obtained as seen in Equation 13. For satisfying the second order optimality condition, the second derivative is taken where we define $\mathbf{H}$ (Hessian) as the second derivative of the cost function $\hat{J}(V_f)$ in the Equation 11. If $\mathbf{H} \in \mathbb{R}^{k \times k}$ is PD then corresponding cost function $\hat{J}(V_f)$ is strictly convex. For PD check, $\mathbf{H} \succ 0$ should be satisfied where $\mathbf{H} \succ 0$ means $x^\intercal \mathbf{H} x > 0$ for every $x \in \mathbb{R}$ with $x \neq 0$ [33].

Let's take the second derivative of the cost function $\hat{J}(V_f)$ in Equation 11:

$$\frac{\partial^2 \hat{J}^n(V_f)}{\partial {V_f}^2} = 2\lambda_a + 2\lambda_P + 2\lambda_s(1-\alpha)(\mathbf{C_x}^\top \mathbf{W_x} \mathbf{C_x} + \mathbf{C_y}^\top \mathbf{W_y} \mathbf{C_y}) = \mathbf{H} \tag{14}$$

Here, x is a nonzero vector and λ_a, λ_p, λ_s, and $(1-\alpha)$ are all positive scalars; so, one should only show that $x^\intercal(\mathbf{C_x}^\top \mathbf{W_x} \mathbf{C_x} + \mathbf{C_y}^\top \mathbf{W_y} \mathbf{C_y})x > 0$ to guarantee that $x^\intercal \mathbf{H} x > 0$ for all nonzero x vectors. This inequality, $x^\intercal(\mathbf{C_x}^\top \mathbf{W_x} \mathbf{C_x} + \mathbf{C_y}^\top \mathbf{W_y} \mathbf{C_y})x > 0$, can be expanded as below into two inequalities after $x^\intercal$ and x are distributed from left and right:

$$\begin{aligned} x^\intercal(\mathbf{C_x}^\top \mathbf{W_x} \mathbf{C_x})x > 0, \quad x^\intercal(\mathbf{C_y}^\top \mathbf{W_y} \mathbf{C_y})x > 0 \\ V_x^\top W_x V_x > 0, \quad V_y^\top \mathbf{W_y} V_y > 0 \end{aligned} \tag{15}$$

where $V_x = \mathbf{C_x} x$ and $V_y = \mathbf{C_y} x$. Here, V_x and V_y are nonzero vectors since x is a nonzero vector and $\mathbf{C_x}$ and $\mathbf{C_y}$ are Toeplitz matrices with nonzero diagonal elements. Subsequently, both inequalities in Equation 15 are satisfied since $\mathbf{W_x}$ and $\mathbf{W_y}$ are all diagonal matrices with positive entries. So, it is shown that cost function $J^{(n)}(V_f)$ given in Equation 11 is strictly convex by the first order and second order optimality tests.

In [29], Aubert and Aujol showed that if $0 < f < 2g$ condition is satisfied then the multiplicative data fidelity term becomes strictly convex. This condition may be violated if off the chart level of smoothing (i.e. large λ_s) is used. However, as suggested in [28] and shown in Figure 3, MAD method employs an iterative approach where images become smoother as iteration proceeds so that deviation of f and g will be minimal in earlier iterations. Therefore, strict convexity conditions will not be violated in earlier iterations, and MAD will get closer to a global minimum before a possible violation of the strict convexity condition. Consequently, global minimum or a minimum in close vicinity of the global minimum is guaranteed.

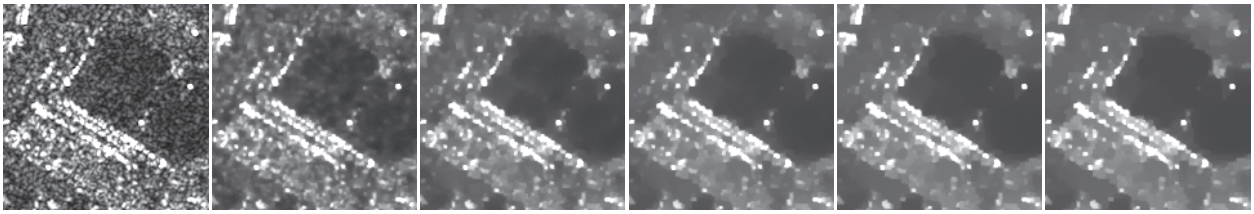

(a) SAR Image (b) Iteration 1 (c) Iteration 2 (d) Iteration 3 (e) Iteration 4 (f) Iteration 5

Figure 3. Generated scale space using the MAD method due to employed iterative minimization approach.

Finally, as an experimental convergence analysis, convergence properties of the original cost function and approximated cost function are analyzed. As seen in Figure 4, the difference between the MAD cost function (Equation 3) and MAD approximated cost function (Equation 11) are decreasing steadily and becomes negligible in the final iteration. This shows that as iteration proceeds, they converge to the same solution within a small error bound which indicates that employed convex relaxation and ℓ_1-norm approximation approaches are successful. Thereby, it can be concluded that original cost function and approximated cost function converges to the same minimum where there may be minimal numerical difference which can be ignored.

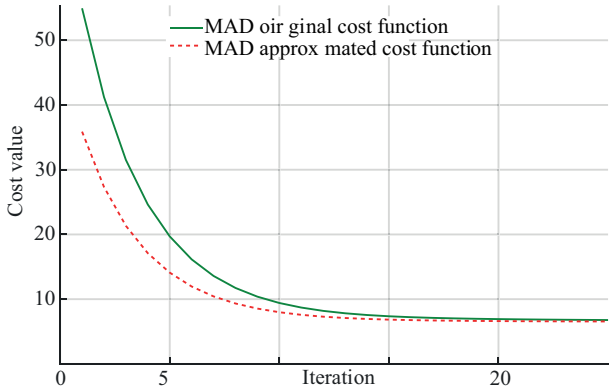

Figure 4. Comparison of original cost function (Equation 3) and its smooth approximation (Equation 11).

3. Experiments and results

In this section, experiments and comparison studies will be presented using synthetically generated SAR images and real-world SAR images. Synthetically generated SAR images are obtained by imposing a different levels of speckle noise onto a test image having geometric shapes with various level of reflectivities. To test despeckling methods with more variety, 10 SAR images with different geographic location, acquisition mode, polarization, resolution, and incidence angle are all downloaded from TerraSAR-X sample imagery as real-world SAR image data set. During tests, parameters of each method are tuned to obtain the best performance. Note that all the experiments are executed using a computer having an Intel i5-3210M 2.5 GHz CPU.

3.1. Performance on synthetic data

Signal-to-noise ratio (SNR) in Equation 16 is used to measure the performance of the proposed method compared to AA, Fast SDD-QL, SRAD, and SAR-BM3D methods.

$$SNR_{db} = 10\log_{10}(P_{signal}/P_{noise}) = 10\log_{10}(A_{signal}/A_{noise})^2 \tag{16}$$

where P is average power, and A_{signal} and A_{noise} operates on signal amplitude and noise amplitude.

Using general speckle model, we synthetically fused speckle noise onto an optical image (Figure 5, a). Then, on that synthetic data, best results of 6 despeckling methods are obtained for each noise level (Figure 5,b). This experiment shows that (a) MAD, SRAD, AA, and Fast SDD-QL methods are successful in general, (b) SAR-BM3D performs best for high noise levels while fails at moderate and low noise levels, (c) Lee performs worse, and (d) proposed MAD method performs satisfactory if all the noise levels are considered. Additionally,

real-world experiments in Section 3.2 shows that SAR-BM3D method fails at high-resolution real-world SAR images although it performs superior in low-noise regime for the synthetically generated data.

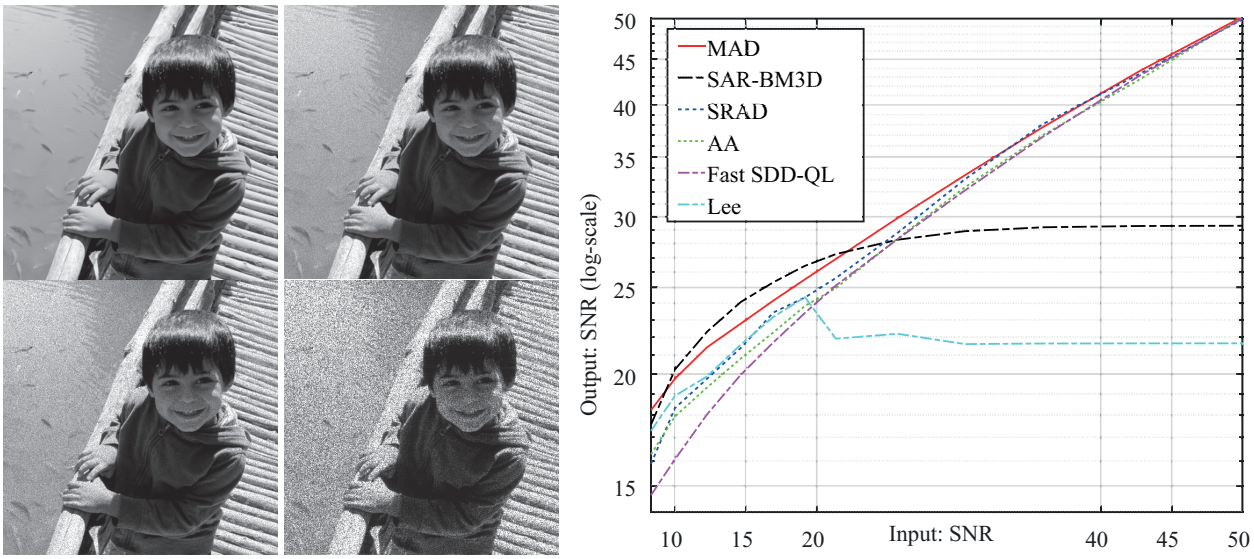

Figure 5. Synthetic image with various speckle noise levels (a) and comparison of the methods (b). Higher SNR value indicates lower noise levels.

3.2. Performance on real-world data

In this section, visual results and execution time comparison will be shown to compare MAD method with other methods (AA, Fast SDD-QL, SRAD, and SAR-BM3D) using real-world TerraSAR-X images which are downloaded from TerraSAR-X Sample Data.

As seen in Figure 6, regions become smoother and more flattened as λ_s increases while point scatterers and edges are preserved for the proposed MAD method. For MAD method, ε controls the approximation accuracy of the TV smoothing term, λ_s controls the smoothing level, and small value for λ_a is chosen for the contribution of additive noise term (i.e. $\lambda_a = 10^{-2}$). Therefore, one should choose values of λ_s, λ_a and ϵ based on the image noise level and desired flatness level in a smoothed image using a training data set as we did so. Note that, execution time of the MAD method increases as ε decreases or λ_s increases.

In Figure 7 despeckling results for Barcelona SAR image is shown. Figure shows that AA method contains dithering artifact due to its unstable explicit solver, SAR-BM3D method blurs the edges, Fast SDD-QL method degrades the image details while MAD and SRAD methods perform better comparing to other methods.

In Figure 8 despeckling results for Dessau SAR image is shown. Figure shows that SAR-BM3D method over-smooths the image, AA and SRAD methods round the edges while MAD and Fast SDD-QL methods perform better comparing to other methods.

In Figure 9 despeckling results for Toronto SAR image is shown. Figure shows that SAR-BM3D method under-smooths the image, AA method degrades the image details, SRAD method over-smooths low-reflectivity regions and also contains dithering artifacts while MAD and Fast SDD-QL methods perform better comparing to other methods.

Figure 7, 8, 9 show that (a) SAR-BM3D method does not perform well in real-world images even though it performs well in synthetic images, especially for high noise levels, (b) SRAD method performs well in some

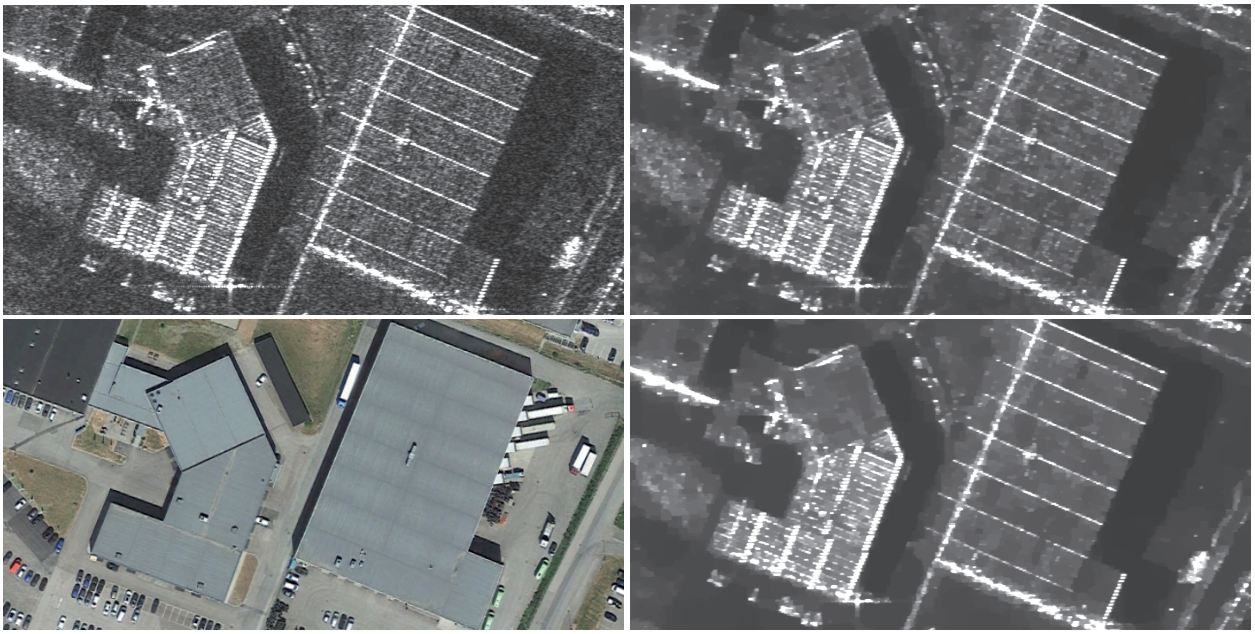

Top left is original SAR image at time t_1 where bottom left is optic image of same location at time t_2
MAD parameters: For top right $\lambda_s = 50$ and for bottom right $\lambda_s = 100$ where $\varepsilon = 10\lambda^{-5}$ and $\lambda_a = 10\lambda^{-2}$

Figure 6. MAD results for Lillestroem (Norway, SpotLight, HH, 0.38 meter).

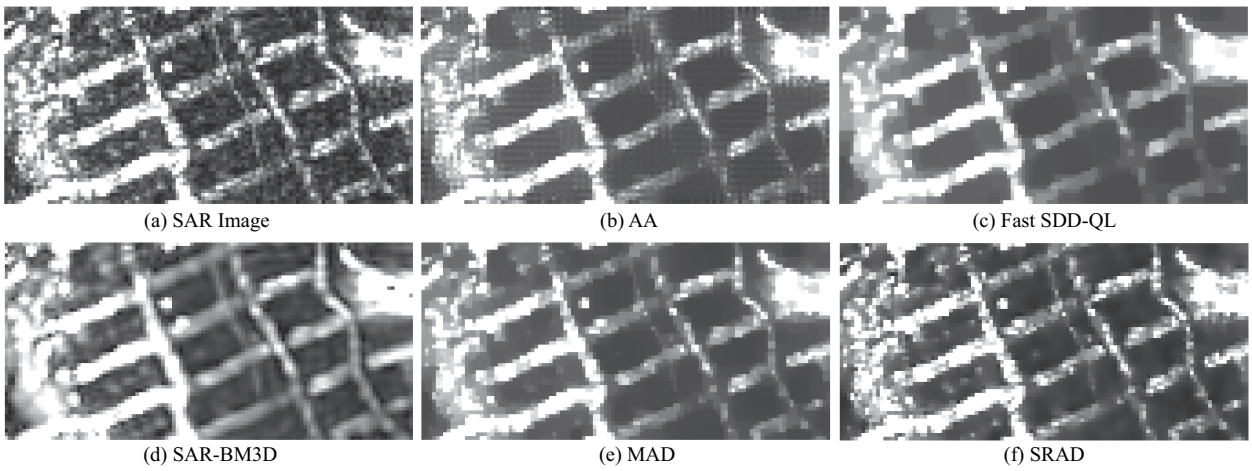

Figure 7. Despeckling results for Barcelona Image (Spain, StripMap, HH, 3 meter).

images but fails in other images and also may contain dithering artifacts, (c) AA method creates dithering artifacts or degrades image details, (d) performance of Fast SDD-QL method is close to performance of the MAD method, and (e) MAD method performs well for all cases and provides superior despeckling performance (better or at least equivalent) comparing to other methods.

Figure 10 shows that SRAD is the fastest despeckling method, while the MAD method is the second fastest one where time difference is marginal. Since SRAD does not provide sufficiently good despeckling performance, MAD is the preferential despeckling method over other methods due to its speed and superior despeckling

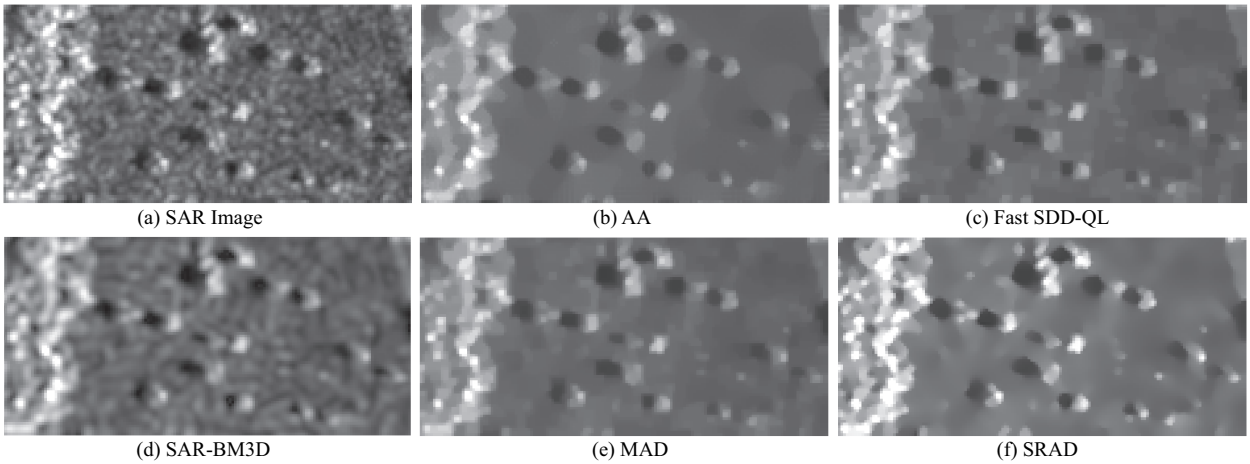

Figure 8. Despeckling results for Dessau Image (Germany, StripMap, HH, 3 meter).

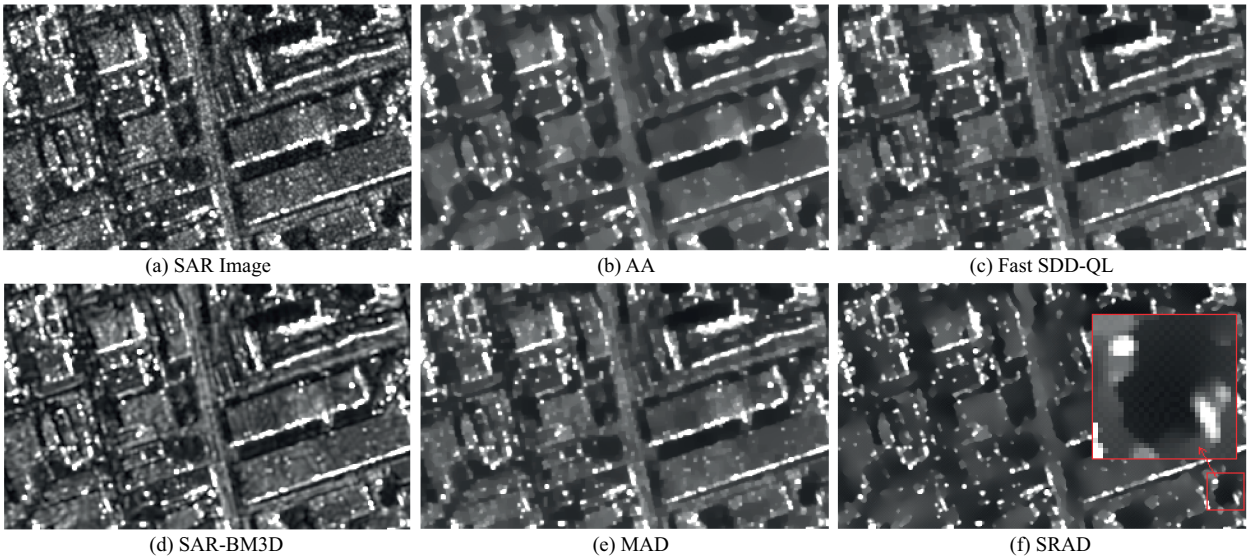

Figure 9. Despeckling results for Toronto Image (Canada, SpotLight, HH, 1 meter).

performance. Although MAD is built on AA method and Fast SDD-QL method, it is faster than both of them. Also, execution time of the MAD and SRAD methods have low variance, which is a nice characteristic.

4. Conclusions

In this study, a novel variational despeckling method, namely multiplicative-additive despeckling (MAD), for SAR images is proposed. Proposed speckle reduction method is constructed as an optimization problem and aims to reduce both multiplicative noise and additive noise simultaneously while preserving image details such as edges and point scatterers. Because of its success in denoising literature, a variational cost function with proper data fidelity terms and a total variation smoothness term is developed. However, proposed variational cost function contains both a nonconvex term and a nondifferentiable term. Therefore, convex relaxation and numerical approximation methods are utilized to obtain a convex and differentiable cost function that is solved

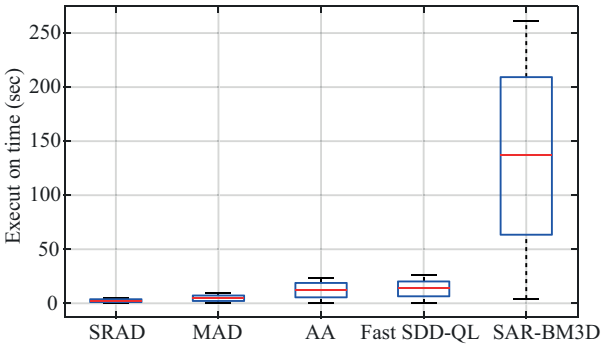

Figure 10. Execution time comparison of all the methods.

in an iterative manner. Consequently, an efficient and stable implicit numerical minimization scheme is obtained. Analyzes of the proposed cost function, its approximation, and the implemented algorithm are presented with its computational and convergence aspects, both theoretically and empirically. Using both synthetically generated SAR images and real-world SAR images, speckle noise reduction performance of the proposed MAD method is compared to the state of the art SAR despeckling methods. Obtained results and comparison studies show that the proposed method provides generally better or at least equivalent despeckling performance compared to existing methods in a stable and computationally efficient manner.

References

[1] Richards JA. Remote Sensing with Imaging Radar. Berlin, Germany: Springer, 2009.

[2] Argenti F, Lapini A, Bianchi T, Alparone L. A tutorial on speckle reduction in synthetic aperture radar images. IEEE Geoscience and Remote Sensing Magazine 2013; 1(3): 6-35. doi:10.1109/MGRS.2013.2277512

[3] Bruniquel J, Lopes A. Multi-variate optimal speckle reduction in SAR imagery. International Journal of Remote Sensing 1997; 18(3): 603-627. doi: 10.1080/014311697218962

[4] Özcan C, Ersoy KO, Oğul İÜ. Fast texture classification of denoised SAR image patches using GLCM on Spark. Turkish Journal of Electrical Engineering & Computer Sciences 2020; 28(1): 182-195. doi: 10.3906/elk-1904-7

[5] Lee JS, Wen JH, Ainsworth TL, Chen KS, Chen AJ. Improved sigma filter for speckle filtering of SAR imagery. IEEE Transactions on Geoscience and Remote Sensing 2009; 47 (1): 202-213. doi: 10.1109/TGRS.2008.2002881

[6] Gonzalez RC, Woods RE. Digital Image Processing. London, UK: Pearson, 2017.

[7] Frost VS, Stiles JA, Shanmugan KS, Holtzman JC. A model for radar images and its application to adaptive digital filtering of multiplicative noise. IEEE Transactions on Pattern Analysis and Machine Intelligence 1982; 4 (2): 157-166. doi: 10.1109/TPAMI.1982.4767223

[8] Lee JS. A simple speckle smoothing algorithm for synthetic aperture radar images. IEEE Transactions on Systems, Man, and Cybernetics 1983; 13 (1): 85-89. doi: 10.1109/TSMC.1983.6313036

[9] Kuan DT, Sawchuk AA, Strand TC, Chavel P. Adaptive noise smoothing filter for images with signal-dependent noise. IEEE Transactions on Pattern Analysis and Machine Intelligence 1985; 7 (2): 165-177. doi: 10.1109/TPAMI.1985.4767641

[10] Lopes A, Touzi R, Nezry E. Adaptive speckle filters and scene heterogeneity. IEEE Transactions on Geoscience and Remote Sensing 1990; 28 (6): 992-1000. doi: 10.1109/36.62623

[11] Lee JS, Jurkevich L, Dewaele P, Wambacq P, Oosterlinck A. Speckle filtering of synthetic aperture radar images: a review. Remote Sensing Reviews 1994; 8 (4): 313-340. doi: 10.1080/02757259409532206

[12] Buades A, Coll B, Morel JM. A review of image denoising algorithms, with a new one. Multiscale Modeling & Simulation 2005; 4 (2): 490-530. doi: 10.1137/040616024

[13] Deledalle CA, Denis L, Tupin F. Iterative weighted maximum likelihood denoising with probabilistic patch-based weights. IEEE Transactions on Image Processing 2009; 18 (12): 2661-2672. doi: 10.1109/TIP.2009.2029593

[14] Parrilli S, Poderico M, Angelino CV, Verdoliva L. A nonlocal SAR image denoising algorithm based on LLMMSE Wavelet shrinkage. IEEE Transactions on Geoscience and Remote Sensing 2012; 50 (2): 606-616. doi:10.1109/TGRS.2011.2161586

[15] Foucher S, Benie GB, Boucher JM. Multiscale MAP filtering of SAR images. IEEE Transactions on Image Processing 2001; 10 (1): 49-60. doi: 10.1109/83.892442

[16] Solbo S, Eltoft T. Homomorphic Wavelet-based statistical despeckling of SAR images. IEEE Transactions on Geoscience and Remote Sensing 2004; 42 (4): 711-721. doi: 10.1109/TGRS.2003.821885

[17] Liu S, Hu Q, Li P, Zhao J, Zhu Z. SAR image denoising based on patch ordering in nonsubsample shearlet domain. Turkish Journal of Electrical Engineering & Computer Sciences 2018; 26 (4): 1860-1870. doi: 10.3906/elk-1711-407

[18] Huang YM, Moisan L, Ng MK, Zeng ZT. Multiplicative noise removal via a learned dictionary. IEEE Transaction on Image Processing 2012; 21 (11): 4534-4543. doi: 10.1109/TIP.2012.2205007

[19] Soganlui A, Cetin M. Dictionary learning for sparsity-driven SAR image reconstruction. In: IEEE International Conference on Image Processing (ICIP); Paris, France; 2014. pp. 1693-1697.

[20] Wang P, Zhang H, Patel M. V. SAR image despeckling using a convolutional neural network. IEEE Signal Processing Letters 2017; 24 (12):1763-1767. doi: 10.1109/LSP.2017.2758203

[21] Lattari F, Leon BG, Asaro F, Rucci A, Prati C et al. Deep learning for SAR image despeckling. Remote Sensing 2019; 11 (13): 1-20. doi: 10.3390/rs11131532

[22] Perona P, Malik J. Scale-space and edge detection using anisotropic diffusion. IEEE Transactions on Pattern Analysis and Machine Intelligence 1990; 12 (7): 629 - 639. doi: 10.1109/34.56205

[23] Weickert J. Anisotropic Diffusion in Image Processing. Stuttgart, Germany: Teubner, 1998.

[24] Yu Y, Acton ST. Speckle reducing anisotropic diffusion. IEEE Transactions on Image Processing 2002; 11 (11): 1260-1270. doi: 10.1109/TIP.2002.804276

[25] Rudin LI, Osher S,Fatemi E. Nonlinear total variation based noise removal algorithms. Physica D: Nonlinear Phenomena 1992; 60 (1): 259-268. doi: 10.1016/0167-2789(92)90242-F

[26] Ozcan C, Sen B, Nar F. Sparsity-driven despeckling for SAR images. IEEE Geoscience and Remote Sensing Letters 2016; 13 (1): 115-119. doi: 10.1109/LGRS.2015.2499445

[27] Nar F. SAR image despeckling using quadratic-linear approximated ℓ_1-norm. Electronics Letters 2018; 54 (6): 387-389. doi: 10.1049/el.2017.3873

[28] Nar F, Atasoy F. Fast quadratic-linear approximated ℓ_1-norm for SAR image despeckling. In: International Conference on Advanced Technologies, Computer Engineering and Science (ICATCES); Karabük, Turkey; 2018. pp. 23-27.

[29] Aubert G, Aujol JF. A variational approach to removing multiplicative noise. SIAM Journal on Applied Mathematics 2008; 68 (4): 925-946. doi: 10.1137/060671814

[30] Durand S, Fadili J, Nikolova M. Multiplicative noise removal using L1 fidelity on frame coefficients. Journal of Mathematical Imaging and Vision 2010; 36 (3): 201-226. doi: 10.1007/s10851-009-0180-z

[31] Bioucas-Dias JM, Figueiredo MAT. Multiplicative noise removal using variable splitting and constrained optimization. IEEE Transactions on Image Processing 2010; 19 (7): 1720-1730. doi: 10.1109/TIP.2010.2045029

[32] Aksoy G, Nar F. Sparsity-driven multiplicative noise reduction. In: Signal Processing and Communications Applications Conference (SIU); Antalya, Turkey; 2017. pp. 1-4.

[33] Nocedal J, Wright SJ. Numerical Optimization. Berlin, Germany: Springer, 2006.